Progress in Natural Science: Materials International 27 (2017) 588–592

HOSTED BY

Contents lists available at ScienceDirect

Progress in Natural Science: Materials International

journal homepage: www.elsevier.com/locate/pnsmi

Original Research

Core loss analysis of Finemet type nanocrystalline alloy ribbon with different thickness

Zhun Li[a,b], Kefu Yao[a,*], Deren Li[b], Xiaojun Ni[b], Zhichao Lu[a,b]

[a] School of Material Science and Engineering, Tsinghua University, No. 20, Shuangqing Rd., Haidian District, Beijing 100084, China
[b] China Iron & Steel Research Institute Group, Advanced Technology and Materials Co., Ltd., No. 76, Xueyuan Nan Rd., Haidian District, Beijing 100081, China

ARTICLE INFO

Keywords:
Nanocrystalline
Ribbon thickness
Core loss
Domain structure

ABSTRACT

Nanocrystalline soft magnetic materials are widely used in power electronic applications due to their high permeability, magnetization and low core loss. In this paper, $Fe_{73.5}Cu_1Nb_3Si_{15.5}B_7$ (at%) nanocrystalline alloy ribbons, with ultra-thin thickness of 14 μm, and also 18 and 22 μm, were prepared by a planar flow casting method with a single roller device. Soft magnetic properties of these ribbons were analyzed after nanocrystallization annealing. The experiments were conducted on toroidal samples using IWATSU B-H Analyzer over a frequency range of 10–100 kHz, at induction amplitudes of 100–500 mT, at room temperature. It was found that the excess eddy current loss P_{ex} was the dominant factor in the overall core loss above 10 kHz. The toroidal samples made of the 14 μm thickness ribbon exhibit very low total core loss of 48 W/kg at a frequency of 100 kHz and magnetic flux density of 300 mT. The ratio of the P_{ex} was up to 89% at 100 kHz. The ribbon with lower thickness exhibits lower P_{ex} and therefore lower total core loss. The domain structure evidences were found. It indicates that the ribbons with small thickness are preferable for application in high frequency condition.

1. Introduction

Nanocrystalline soft magnetic materials are widely used in power electronic applications. With the development of electronic and information technology to high-frequency, digital and integrated direction, the working frequency of the core is getting higher and higher [1–4]. In order to reduce system energy consumption, to achieve energy saving and environmental protection purpose, magnetic materials with lower core loss soft were in demand.

Many researches have been carried out on the core loss of crystalline alloys, such as silicon steel [5], MnZn ferrite [6], and amorphous alloys [7]. There are several ways to reduce the overall core loss of the amorphous alloy ribbon. Some research works were focused on increasing the saturation magnetic induction [8–10]. Ogawa et al. [11] studied a new Fe-based amorphous ribbon with a commercial name of HB1. It had a high saturation magnetic induction of 1.64 T which was improved by 0.07 T over an Fe-based amorphous material of Metglas 2605SA1 (SA1) alloy. The core loss for the new material at 50 Hz, 1.4 T was about 0.065 W/kg which was superior to the SA1 alloy by 15%. The heat treatment has important impact on the core loss of the nanocrystalline alloy [12]. Han et al. [13] studied the impact of heat-treatment on the coercivity, permeability and core loss properties of $Fe_{73.5}Cu_1Nb_3Si_{15.5}B_7$ nanocrystalline alloy ribbon, it was found that compared with the traditional so-called one-step annealing, the two-step annealing that made the samples pretreated at 400 ℃ and nanocrystallized at 560 ℃ for 1 h exhibit excellent magnetic properties, such as lower coercive force of 0.7 A/m, higher initial permeability of 9.16×10^4, lower core loss of 0.18 W/kg at 0.7 T and 400 Hz, and 0.5 W/kg at 0.7 T and 1 kHz, respectively. Since the classical eddy current loss is positively correlated with the ribbon thickness, some previous work on making the thinner ribbon [14] was carried out.

It is known that the core loss of the magnetic cores could be separated into three portions due to the nature of the loss mechanism. They are the static hysteretic loss P_h, the classical eddy current loss P_{ec} and the excess eddy current loss P_{ex} (or anomalous loss) [15–20]. The static hysteretic loss is determined by the measurement of the quasi-static hysteresis loop. The classical eddy current loss could be calculated from the fundamental equations of electromagnetics and the applied sinusoidal field, together with considering the skin effect. The excess eddy current loss is attributed to the non-sinusoidal non-uniform and non-repetitive domain wall motion [21] and determined by the total core loss P_t minus the hysteretic loss and the eddy current

Peer review under responsibility of Chinese Materials Research Society.
* Corresponding author.
E-mail address: kfyao@tsinghua.edu.cn (K. Yao).

http://dx.doi.org/10.1016/j.pnsc.2017.09.002
Received 30 March 2017; Received in revised form 10 September 2017; Accepted 11 September 2017
Available online 06 October 2017

loss. Then, understanding the separated core losses would be helpful for us to understand the overall loss better.

In this paper, the Fe-based nanocrystalline alloy ribbons, with ultra-thin thickness of 14 μm and also conventional thickness of 18 and 22 μm, were prepared using a planar flow casting method, and the technique of the separation of the core loss was applied to a group of nanocrystalline ribbons with different thickness. The dominant loss characteristics in different frequency range has been studied. And the domain structure of the ribbons has been examined.

2. Experiment

In this work, alloy ingots with nominal composition of $Fe_{73.5}Cu_1Nb_3Si_{15.5}B_7$ were prepared by induction melting of the mixture of industrial-purity metals of Fe (99.9 mass%), Cu (99.9 mass%), Si (99.9 mass%), pre-alloyed Nb-Fe (99.7 mass%) and Fe-B (99.7 mass%) in a high vacuum condition. $Fe_{73.5}Cu_1Nb_3Si_{15.5}B_7$ (at%) soft magnetic alloy ribbons with 14, 18 and 22 μm in thickness were prepared by a planar flow casting method using a single wheel. The density of the alloy was 7200 kg/m^3. These ribbons were wounded into toroidals having an outer diameter, an inner diameter and a height of 25, 16, and 10 mm, respectively.

These cores were annealed at 550 ℃ for 1 h in a furnace under 2 L/min flowing argon and 250 Oe transverse magnetic field. The starting point of the applied magnetic field was controlled that from the cores cooled to 400 ℃, the end of insulation of 550 ℃ and the very beginning of the annealing. These three kinds of annealing were marked asI, II and III. The B-H loops and the total core losses were studied. The separation of losses technique had been applied to these cores.

The initial permeability, coercivity and quasi-static hysteresis loop was measured using a static magnetic property analyzer (MATS-2010SD). The testing was carried out at room temperature with maximum magnetic field values of 1, 2, 3, 5, 8 and 10 A/m.

IWATSU B-H Analyzer was used to measure the core losses of the samples between 10 and 100 kHz with a sinusoidal magnetic induction. The maximum flux density values were 100, 200, 300, 400 and 500 mT.

The magnetic domain structures of the annealed ribbons with different thickness were analyzed with the Zeiss AX10 magneto optic Kerr microscope.

3. Results and discussion

The B-H loops of the cores annealed at 550 ℃ with different start point of 250 Oe transverse magnetic field (H) are shown in Fig. 1. The B-H loop of the cores which annealed with longer time of transverse magnetic field applied shows better linear, in another word, the permeability of these cores, which can be calculated by dB/dH, is nearly constant until getting saturated. The saturation point of the B-H loop is about 25 A/m. The following results are based on the III type

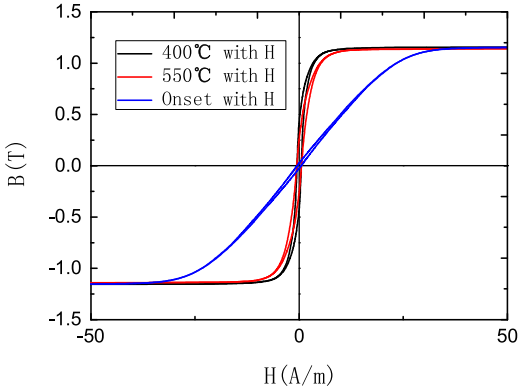

Fig. 1. B-H loops for cores annealed with transverse magnetic field (H) start from cooling to 400 ℃, insulation of 550 ℃ and the onset of the annealing.

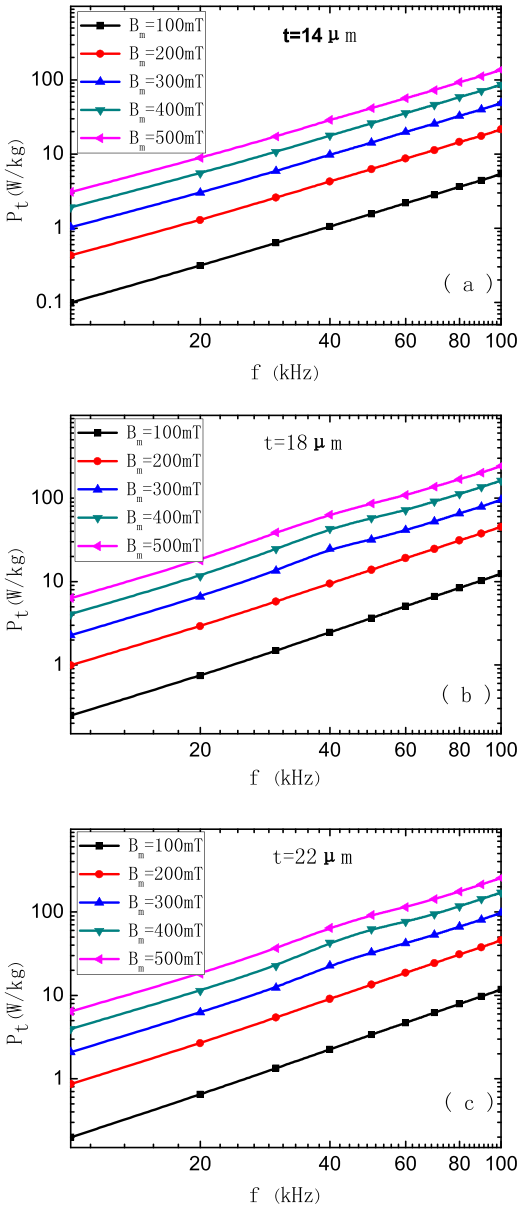

Fig. 2. The total core loss for annealed ribbons with thickness of (a) 14 μm, (b) 18 μm, and (c) 22 μm as a function of switching frequency at various constant maximum flux density.

annealing.

Fig. 2 shows the measured total core loss P_t, of the toroidal samples made of 14, 18 and 22 μm ribbons, per cycle for a series of maximum applied flux densities. It is obviously that the total core loss increases with the rising of the amplitude and frequency of the induction.

Fig. 3 shows the total core loss of three kinds of toroidal samples. The results were measured at 10–100 kHz and the induction amplitude was 300 mT. The total core loss of the core made of 14 μm ribbons under this condition was 48 W/kg, as a contrast, the core losses of the cores made of 18 and 22 μm ribbons were 61 and 81 W/kg, respectively. It shows that the upward trend of the total core loss for thin ribbon was much more moderate then the ribbons with thick thickness. Then the separation of the losses has been carried out, which might provide the insight into the cause of the difference in the total core losses of the three kinds of samples [22–24].

These results agree with Yoshizawa's work [25]. In his work, the thickness dependence of the magnetic properties was studied. The FINEMET type cores with different thickness were annealed with

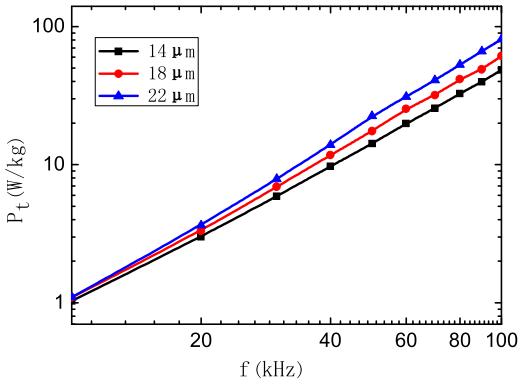

Fig. 3. Total core loss of the cores made of annealed ribbons with different thickness as a function of switching frequency at 300 mT.

longitudinal and transverse magnetic field applied and also with no magnetic field applied. Both of these three kinds of cores show a rising core loss with the thickness increased. The samples subjected to transverse field annealing had especially low core loss. The core loss of 22 μm ribbon was about 70 W/kg. Trupp et al. [26] took a study on the effect of ribbon thickness on power loss and high frequency behavior of Finemet type cores. A classical eddy current loss formula was applied to analyze the core loss property. Two kinds of cores were made of the ribbon with thickness of about 16 and 20 μm. Both of these two kinds of cores exhibited a rising trend of core loss with the rising of frequency and the amplitude of the induction, and also the core loss of the cores made of thinner ribbon was lower. The core loss at a frequency of 100 kHz and induction of 300 mT was about 50 and 70 W/kg for the cores made of 16 and 20 μm ribbons, respectively.

As shown in Fig. 4, the static hysteretic loss P_h varies with the maximum magnetic-flux intensity (B_m), following the formula (1):

$$P_h = P_0 B_n^m, \tag{1}$$

where m = 1.544, P_0 is a fitting parameter for the hysteretic loss in W/kg, and P_0 is 70×10^{-6}, 75×10^{-6} and 135×10^{-6} for the core made of 14, 18 and 22 μm ribbons, respectively. The Eq. (1) agrees well to the previous work of Ref. [23].

The coercivity (H_c), initial permeability (μ_i), maximum magnetic induction at 800 A/m (B_{800}) and anisotropy constant (K_u) properties of these three thickness ribbons, which were annealed at 550 ℃ for 1 h with 250 Oe transverse magnetic field, are shown in Table 1 as bellow. The ribbon with smaller thickness shows lower H_c and μ_i, and the magnetic anisotropy constant is bigger.

The eddy current losses were calculated in loss per cycle for the case when the thickness of the lamination is much greater than the skin depth. Under constant permeability and sinusoidal applied field

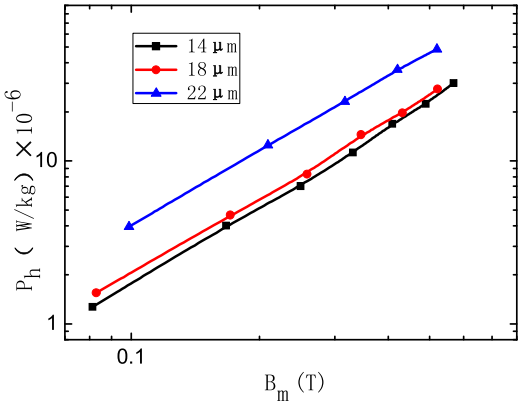

Fig. 4. Static hysteretic loss per cycle of the annealed ribbons as a function of maximum flux density.

Table 1
Magnetic properties of the ribbon with different thickness.

Ribbon thickness (μm)	Hc (A/m)	μ_i (10^4)	B_{800}	K_u (J/m ^{3})
14	0.65	4.1	1.18	18.2
18	0.72	4.1	1.18	18.1
22	0.75	4.2	1.18	17.9

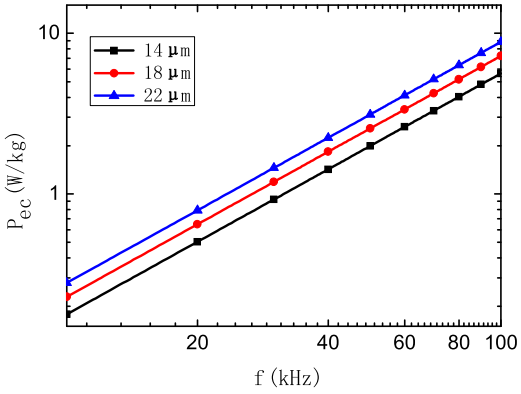

Fig. 5. Eddy current loss per cycle of the annealed ribbons as a function of switching frequency.

conditions, the classical eddy current loss P_{ec} follows the Eq. (2):

$$P_{ec} = \frac{\pi^{3/2} t B_m^2 f^{3/2}}{2\rho\sqrt{\mu\rho_e}}, \tag{2}$$

where t is the ribbon thickness, μ is the permeability of the sample, ρ_e is the resistivity (115 μΩ m), ρ is the density of the material, and f is the switching field frequency. The eddy current loss curves are shown in Fig. 5. The P_{ec} values at 100 kHz and 300 mT are 5.6, 7.2 and 8.4 W/kg for the cores made of 14, 18 and 22 μm ribbons, respectively. The rising trend of the eddy current losses exhibits no difference under this model.

The excess eddy current loss was then calculated. Since the static hysteretic loss is very small, the excess eddy current loss value can be obtained by the equation as follow

$$P_{ex} = P_t - P_{ec}. \tag{3}$$

The excess eddy current loss curves which measured at 300 mT and the frequency range of 10–100 kHz are shown in Fig. 6. It fits the equation

$$P_{ex} = P_0' f^n, \tag{4}$$

where P_0' is a fitting parameter for the excess eddy current loss in W/kg, f is the switching field frequency. Fitting of the curves provide the parameters P_0' = 0.0112, 0.0123, 0.0091, and n = 1.79, 1.82, 1.95 for the cores made of 14, 18 and 22 μm ribbons, respectively. The ratio of the excess eddy current losses to the total losses is illustrated in Fig. 5. The P_{ex} value and the ratio of P_{ex} for these three kinds of ribbon rising with the increase of the frequency, and P_{ex} was almost the same of 0.8 W/kg at 10 kHz, and with the frequency rising the P_{ex} value at 100 kHz with the induction of 300 mT is 43, 54, 72 W/kg for the cores made of 14, 18 and 22 μm ribbons, respectively. The ratio of the excess eddy current loss was bigger when the thickness of the ribbon was smaller within 60 kHz, and with the frequency rising the ratio of P_{ex} for these ribbons was nearly the same. The ratio was up to 89% at 100 kHz, and this value is agree to the previous work of Refs. [21,23], which illustrated the ratio of the excess eddy current loss at 100 kHz can be up to 70–90%.

The magnetic domain structure was examined by using the ZEISS AX10 Magneto-optical Kerr microscope. The domain structures of the ribbons with thickness of 14, 18 and 22 μm which were annealed under

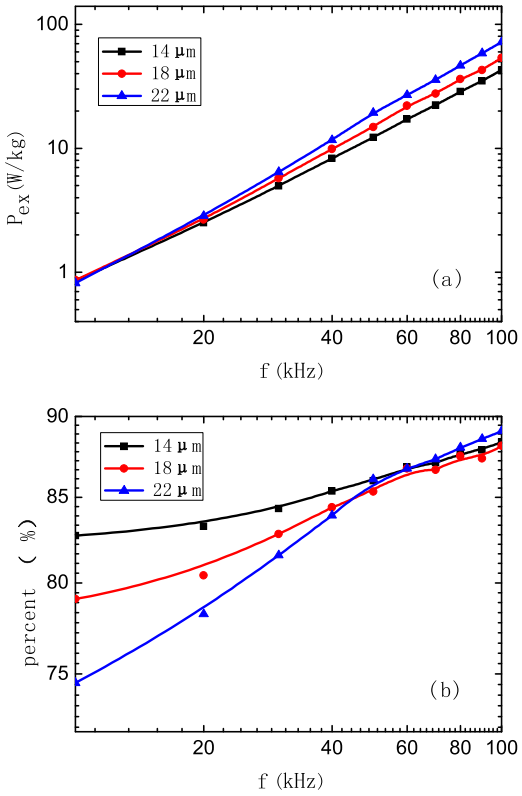

Fig. 6. Excess eddy current loss of the annealed ribbons as a function of switching frequency, the ratio of excess eddy current loss to total loss.

transverse magnetic field at 550 °C for 1 h are shown in Fig. 7. It can be found that the main domains are wide and separated by 180° walls, some parts of the ribbon with the thickness of 14 μm has the labyrinthine domain, which has not been found in the ribbons with the thickness of 18 and 22 μm. The domain width of the ribbon with 22 μm in thickness is larger than that in the 18 μm ribbon. So there are more domain walls per unit volume in the ribbon with smaller thickness. Yoshizawa [25] pointed out that the domain structure would be changed due to the ribbon sample thickness, induction amplitude and other conditions and parameters. We have found an evidence for this assume. The magnetic direction is illustrated by the white arrow in Fig. 7. It indicates that the ribbon exhibits transverse anisotropy.

The domain width decreases with the decrease of the ribbon thickness, and the average domain width w can be estimated as [27–29]

$$w \approx \sqrt{\frac{2\gamma_w t}{K_u \cdot (N_{zz}\sin^2\beta + N_{yy}\cos^2\beta)}}, \tag{5}$$

where γ_w is the domain wall energy, t is the ribbon thickness, $K_u = H_k J_s/2$ is the anisotropy constant, J_s is the saturation magnetization, β is the out-of-plane angle of the magnetization vector, N_{zz} (≈ 1) is the demagnetizing factor normal to the ribbon plane and N_{yy} (≈ 0.004) is the demagnetizing factor across the ribbon width. For the ribbon with transverse anisotropy $\beta = 0°$, the domain width is proportional to $(t/K_u)^{1/2}$. The domain widths of the annealed ribbons were 165, 200 and 230 μm for the ribbon thickness of 14, 18 and 22 μm, respectively. And this is agree to the theoretical calculated domain width ratio value of 0.88:1:1.12, which is derived from the ratio of $(t/K_u)^{1/2}$.

According to Herzer's theory [27–29], the total eddy current loss (include classic eddy current loss and excess eddy current loss), has the form of

$$P_t \approx P_{ec}\left(1 + \frac{w^2}{(w\cos\beta + t)^2}\frac{m^2}{1-m^2}\right), \tag{6}$$

where m denotes the average magnetization component along the ribbon axis normalized to the saturation magnetization. The excess eddy current loss (micro-eddy current loss) P-P_{ec} associated with the rotation of the magnetization vector within a domain. The ratio of excess eddy current loss to the total loss has the form of

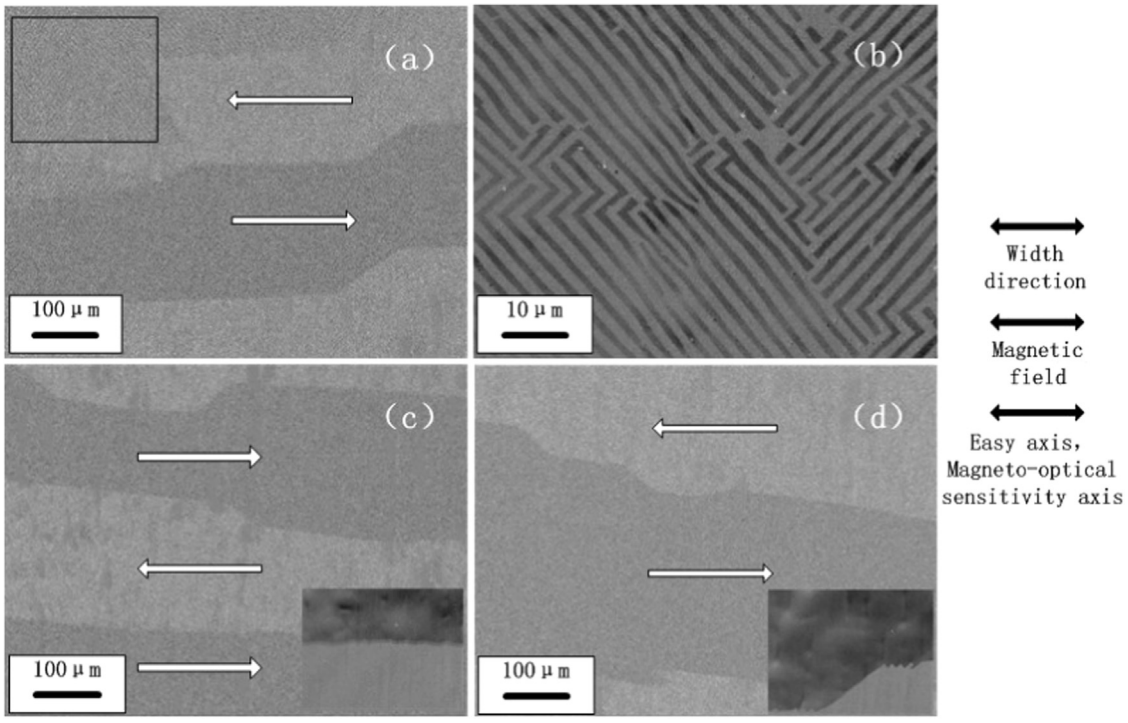

Fig. 7. Magnetic domain structure of the annealed ribbon with different thickness, (a) t = 14 μm, (b) partial enlarged view of black box part of (a), (c) t = 18 μm, (d) t = 22 μm, and the inset at the lower right corner of (c) and (d) is the 10 times partial enlarged view of the same area, respectively.

$$P_{ex}/P_t = \frac{2\gamma_w m^2}{2\gamma_w + (\sqrt{8K_u\gamma_w t + t})(1 - m^2)}. \quad (7)$$

It can be derived that the ratio increases with the decreasing of the ribbon thickness. The calculation results proves that the ratio of P_{ex} at 10 kHz and B_m = 300 mT are 82.7%, 79.1%, and 74.5% for t = 14, 18, and 22 μm, respectively.

In Bertotti's model [30], the energy dissipation in materials under alternating magnetic field is due to eddy currents generated during motion of the magnetic domain [31], and the motion is no-sinusoidal, non-uniform and non-repetitive [23]. The principal reason for the difference of P_{ex} is the domain structure. In this model, the domain structure was considered as n magnetic objects, randomly placed in the sample cross section S, and assuming $n(t)$ is the number of magnetic objects involved in the process of magnetization. A fraction of the external field required for field compensation derived from eddy currents generated by these magnetic objects could be written as following

$$H_{ex} = P_{ex}/(4B_m f) = 4\sigma G^{(w)} S B_m f/n, \quad (8)$$

where σ is the electrical conductivity, $G^{(w)}$ is a dimensionless coefficient, and it takes a constant value of 0.1356 when consider a case where all of the switching of the magnetization occurs at a single 180° domain wall.

We can derive from the Eq. (8) and some other previous work that the larger number of the domain walls the smaller P_{ex} is [32,33]. The P_{ex} is proportional to the square of B_m and f, so the P_{ex} of 14 μm ribbon which has more domain wall is smaller than 18 and 22 μm ribbon from10 kHz. In fact, within the fitting expression of the excess loss (Eq. (4)), the index of the frequency for the core made of thinner ribbon is smaller, and therefore the P_{ex} upward trends with f of 14 μm ribbon is much more moderate. This is the dominant factor of the upward trends of the overall core losses. It indicates that small thickness is preferable to be applied in high frequency condition.

4. Conclusion

Nanocrystalline ribbons with the thickness of 14, 18, and 22 μm were prepared by planar flow casting technique, and the cores made of these three kinds of ribbons were nano-crystallization annealed then. The total loss at 300 mT and 100 kHz of the ribbon with a ultra-thin thickness of 14 μm is only 48 W/kg. The separation of losses technique was applied. The ratio of P_{ex} is up to 89% at 100 kHz with the induction of 300 mT. So the P_{ex} is the dominant factor of the total loss above 10 kHz. The magnetic domain structure is refined with the decrease of the thickness of the ribbon, so the ribbon with smaller thickness exhibits lower P_{ex}, and therefore the total core loss is lower.

Acknowledgment

This work was supported by the National Key Basic Research and Development Programme (Grant no. 2016YFB0300502).

References

[1] Y. Naitoh, T. Bitoh, T. Hatanai, A. Makino, A. Inoue, T. Masumoto, Nanostruct. Mater. 8 (1997) 987–995.
[2] R. Hasegawa, Mater. Sci. Eng. A 375–377 (2004) 90–97.
[3] A.D. Setyawan, K. Takenaka, P. Sharma, M. Nishijima, N. Nishiyama, A. Makino, J. Appl. Phys. 117 (2015) 17B715.
[4] G. Herzer, Acta Mater. 61 (2013) 718–734.
[5] T. Iuchi, S. Yamaguchi, T. Ichiyama, M. Nakamura, T. Ishimoto, K. Kuroki, J. Appl. Phys. 53 (1982) 2410–2412.
[6] M. Lauda, J. Füzer, P. Kollár, M. Strečková, R. Bureš, J. Kováč, M. Baťková, I. Baťko, J. Magn. Magn. Mater. 411 (2016) 12–17.
[7] D.R. Li, L. Zhang, G.M. Li, Z.C. Lu, S.X. Zhou, Prog. Nat. Sci. Mater. 22 (2012) 244–249.
[8] A. Makino, H. Men, T. Kubota, K. Yubuta, A. Inoue, Mater. Trans. 50 (2009) 204–209.
[9] J.F. Li, X. Liu, S.F. Zhao, H.Y. Ding, K.F. Yao, J. Magn. Magn. Mater. 386 (2015) 107–110.
[10] R. Xiang, S.X. Zhou, B.S. Dong, G.Q. Zhang, Z.Z. Li, Y.G. Wang, C.T. Chang, Prog. Nat. Sci. Mater. 24 (2014) 649–654.
[11] Y. Ogawa, M. Naoe, Y. Yoshizawa, R. Hasegawa, J. Magn. Magn. Mater. 304 (2006) e675–e677.
[12] C. Beatrice, C. Appino, E. Ferrara, F. Fiorillo, J. Magn. Magn. Mater. 160 (1996) 302–304.
[13] Y. Han, A.D. Wang, A.N. He, C.T. Chang, F.S. Li, X.M. Wang, J. Mater. Sci. – Mater. Electron. 27 (2016) 3736–3741.
[14] D.R. Li, L. Zhang, G.M. Li, Z.C. Lu, S.X. Zhou, Prog. Nat. Sci. 22 (2012) 244–249.
[15] T. Rahman, J.C. Akiror, P. Pillay, D.A. Lowther, in: Proceedings of the Compumag Parameters, IEEE, Budapest, 2013, pp. 4–5.
[16] G. Bertotti, F. Fiorillo, G.P. Soardo, IEEE Trans. Magn. Mag. 23 (1987) 3520–3522.
[17] D. Lin, P. Zhou, W.N. Fu, Z. Badics, Z.J. Cendes, IEEE Trans. Magn. Mag. 40 (1987) 1318–1321.
[18] G. Bertotti, IEEE Trans. Magn. Mag. 24 (1988) 621–630.
[19] O. Bottauscio, F. Fiorillo, C. Beatrice, A. Caprile, A. Magni, IEEE Trans. Magn. Mag. 51 (2015) 2800304.
[20] P. Kollár, Z. Birčáková, J. Füzer, R. Bureš, M. Fáberová, J. Magn. Magn. Mater. 327 (2013) 146–150.
[21] K.J. Overshott, IEEE Trans. Magn. Mag. 17 (1981) 2698–2700.
[22] G. Bertotti, J. Appl. Phys. 57 (1985) 2110–2117.
[23] M.A. Willard, T. Francavilla, V.G. Harris, J. Appl. Phys. 97 (2005) 10F502.
[24] Y. Zhang, M.C. Cheng, P. Pillay, in: Proceedings of the IAS, IEEE, Houston, 2009, pp. 1–5.
[25] Y. Yoshizawa, K. Yamauchi, JANIEEE Trans. Magn. 5 (1990) 1070–1076.
[26] Tobias Trupp, Zoltán Palánki, ⟨http://www.magnetec.de/fileadmin/pdf/smm21_ttr.pdf⟩.
[27] C. Kittle, Rev. Mod. Phys. 21 (1949) 541–583.
[28] G. Herzer, J. Magn. Magn. Mater. 254–255 (2003) 598–602.
[29] G. Herzer, United Patent 6,011,475, 2000.
[30] G. Bertotti, F. Fiorillo, P. Mazzetti, J. Magn. Magn. Mater. 112 (1992) 146–149.
[31] C.D. Graham Jr, J. Appl. Phys. 53 (1982) 8276–8280.
[32] S. Flohrer, R. Schäfer, J. McCord, S. Roth, L. Schulz, G. Herzer, Acta Mater. 54 (2006) 3253–3259.
[33] S. Flohrer, R. Schäfer, J. McCord, S. Roth, L. Schulz, F. Fiorillo, W. Günther, G. Herzer, Acta Mater. 54 (2006) 4693–4698.